

Room-temperature InP distributed feedback laser array directly grown on silicon

Zhechao Wang^{1,2†}, Bin Tian^{1,2†}, Marianna Pantouvaki³, Weiming Guo³, Philippe Absil³, Joris Van Campenhout³, Clement Merckling³ and Dries Van Thourhout^{1,2*}

Fully exploiting the silicon photonics platform for large-volume, cost-sensitive applications requires a fundamentally new approach to directly integrate high-performance laser sources using wafer-scale fabrication methods. Direct-bandgap III-V semiconductors allow efficient light generation, but the large mismatch in lattice constant, thermal expansion and crystal polarity makes their epitaxial growth directly on silicon extremely complex. Using a selective-area growth technique in confined regions, we surpass this fundamental limit and demonstrate an optically pumped InP-based distributed feedback laser array monolithically grown on (001)-silicon operating at room temperature and suitable for wavelength-division-multiplexing applications. The novel epitaxial technology suppresses threading dislocations and anti-phase boundaries to a less than 20-nm-thick layer, which does not affect device performance. Using an in-plane laser cavity defined using standard top-down lithographic patterning together with a high yield and high uniformity provides scalability and a straightforward path towards cost-effective co-integration with silicon photonic and electronic circuits.

The potential of leveraging well-established and high-yield manufacturing processes developed initially by the electronics industry has been the main driver fuelling the massive research into Si photonics over the last decade^{1–6}. In particular, for very high-volume applications such as optical interconnects in chip-to-chip or even on-chip communication links (required for resolving the interconnect bottleneck), a platform that fully benefits from the economies of scale offered by processing in advanced CMOS foundries is essential to reduce costs. From the start of its development, however, a lack of efficient optical amplifiers and laser sources monolithically integrated with the Si platform inhibited its widespread adoption in high-volume applications. Solutions relying on flip-chipping prefabricated laser diodes^{7,8} or bonding III-V epitaxial material^{9–11} are now being deployed in commercially available optical interconnects, but are less compatible with standard high-volume and low-cost manufacturing processes. Approaches focusing on the engineering of group IV materials or their alloys have achieved optical gain, but still require extensive work to achieve room-temperature lasing with reasonable efficiency^{12–15}.

Accordingly, the monolithic integration of direct-bandgap III-V semiconductors (well known to be efficient light emitters but now also heavily studied as a replacement gate material for future CMOS nodes¹⁶) with the Si photonics platform is under intense investigation. However, considerable hurdles need to be overcome. When directly growing III-V semiconductors on Si substrates, the large lattice mismatch ($\varepsilon_{\text{InP/Si}} = 8.06\%$), the difference in thermal expansion and the different polarity of the materials result in large densities of crystalline defects, including misfit and threading dislocations, twins, stacking faults and anti-phase boundaries, strongly degrading the performance and reducing the lifetime of any device fabricated in the as-grown layers¹⁷. Several routes to overcome these issues have been proposed. GaP-related materials can be grown on (001)-Si substrates with a small lattice mismatch, and pulsed laser oscillation around 980 nm up to 120 K (ref. 18) has

been achieved, but shifting the laser wavelength towards the telecommunication band remains challenging. GaSb, although strongly lattice-mismatched with Si, can be integrated on Si with a relatively low density of threading or screw dislocations ($\sim 10^5$ – 10^6 per cm^2), and room-temperature laser operation has been demonstrated¹⁹. However, the relatively thick buffer layer hinders co-integration with electronic or photonic integrated circuits. Good thermal stability and high output power have been demonstrated for InAs quantum dot lasers embedded in a thick GaAs buffer^{20,21}, but the few-degree miscut Si substrate together with the thick III-V buffers needed to accommodate the lattice mismatch are not compatible with standard CMOS processes. Finally, the growth of III-V nanowires on Si has been studied extensively^{22,23}, but it is challenging to integrate these with low-loss optical waveguide circuits.

Recently, the field of III-V epitaxy on Si received a boost by the renewed interest of the electronics industry in using high-mobility compound semiconductors in next-generation CMOS^{16,24}. Low-defect-density growth of GaAs²⁵, InP^{26,27} and InGaAs²⁸ compounds using selective-area growth on pre-patterned (001)-Si was achieved, demonstrating the world's first III-V FinFET devices on a 300 mm substrate fully processed in a production Si CMOS line. Here, we leverage this process to demonstrate room-temperature laser operation of wafer-scale integrated InP lasers directly grown on standard (001)-Si substrates. Starting with millimetres-long InP waveguides of high optical quality grown selectively onto a Si substrate and using standard top-down integration processes, including the definition of gratings on top of these waveguides, we fabricated distributed feedback lasers (DFB) exhibiting robust single-mode operation. We demonstrate an array of DFB lasers with well-controlled emission wavelengths, illustrating the uniformity of the III-V material and devices and showing its promise for high-capacity wavelength division multiplexing (WDM) applications. The in-plane configuration and the use of a selective-area growth technique directly on standard (001)-Si substrates facilitate

¹Photonics Research Group, Ghent University-imec, Sint-Pietersnieuwstraat 41, Ghent 9000, Belgium. ²Center for Nano- and Biophotonics (NB-Photonics), Ghent University, Sint-Pietersnieuwstraat 41, Ghent 9000, Belgium. ³IMEC, Kapeldreef 75, 3001 Heverlee, Belgium. [†]These authors contributed equally to this work. *e-mail: dries.vanthourhout@intec.ugent.be

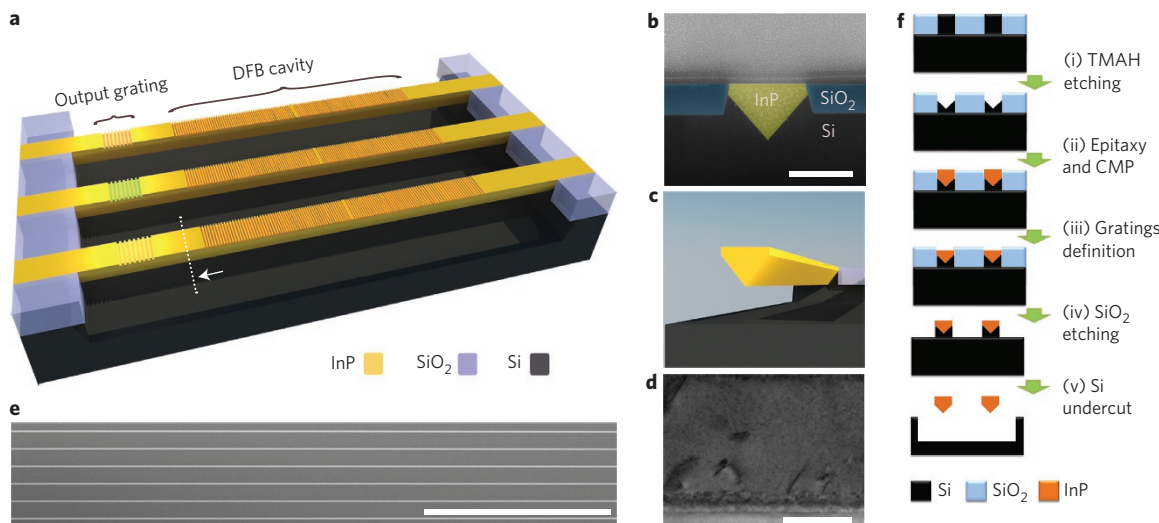


Figure 1 | Monolithic integration of InP lasers on Si. **a**, Schematic of the monolithically integrated InP DFB lasers on Si. The laser cavities and the output gratings are labelled. Differently coloured output gratings illustrate the tunability of the lasing wavelength. **b**, False-coloured SEM cross-section view of an InP-on-Si waveguide. Scale bar, 500 nm. **c**, Schematic cross-section plot of the diamond-shaped waveguide, at the position indicated by a dotted line in **a**. **d**, TEM image of a specimen prepared parallel to the InP-on-silicon waveguide. Scale bar, 200 nm. **e**, SEM top view of an array of InP-on-Si waveguides. Scale bar, 10 μ m. **f**, Integration flow steps. Cross-sections are shown orthogonal to the laser axis following each separate process step.

future integration of this DFB laser array with both photonic and electronic circuits.

Fabrication

Figure 1a schematically depicts the fabricated DFB laser array. Each laser consists of a high-quality InP waveguide, on top of which first-order gratings are defined with a $\lambda/4$ phase shift section inserted in the centre. To facilitate characterization of the devices, second-order gratings coupling the light out of the laser bar vertically were defined 30 μ m away from the DFB cavities. Because the InP is directly grown on Si and its bandgap energy (1.35 eV @ 300 K) is higher than that of Si (1.12 eV @ 300 K), all light generated in the III-V material will be absorbed directly in the substrate when pumping the as-grown structures. The Si substrate beneath the InP-based laser device was thus etched away intentionally. The suspended laser cavity was supported by two Si pedestals outside the laser cavity. Figure 1b presents a scanning electron microscope (SEM) cross-section view of a single waveguide before the Si substrate was undercut. The InP is 500 nm wide at the top and the thickness of the SiO₂ layer next to the waveguide is 250 nm. Note the particular diamond shape of the InP waveguide, which is a consequence of the epitaxial process used²⁹. Figure 1f (steps i and ii) briefly summarizes the epitaxy process flow. The starting substrate was a 300 mm (001)-Si wafer on which 500-nm-wide ridges planarized with SiO₂ were defined in a standard shallow-trench-isolation (STI) process. The Si ridges were selectively etched away using a tetramethylammonium hydroxide (TMAH) solution (5% @ 80 °C), forming a V-groove composed of two flat {111} planes at the bottom of the resulting trench²⁹. The subsequent InP selective-area growth inside this trench was carried out in a metal–organic chemical vapour phase epitaxy (MOVPE) reactor and consisted of a low-temperature nucleation step followed by higher-temperature growth, as described in the Methods. This second step was continued until the InP protruded above the SiO₂ mask, after which the top surface was planarized by a chemical-mechanical-polishing (CMP) process. A top-view SEM image of the grown waveguide array taken after this step is presented in Fig. 1e. These uniform waveguides can be several millimetres long.

Given the 8% lattice mismatch as well as the 84% difference in thermal expansion coefficient, growing InP directly on Si typically results in a large density of misfit and threading dislocations, which

are detrimental for optoelectronic devices¹⁷. A common approach to accommodate the mismatch makes use of a several-micrometre-thick buffer layer^{30–32}. However, such a thick buffer layer inhibits integration with Si electronic or photonic devices fabricated on the same wafer. In the present approach, the thickness of this defective nucleation layer could be limited to ~20 nm. Nevertheless, and despite the very large lattice mismatch, the transmission electron microscope (TEM) image in Fig. 1d shows that the resulting InP waveguide is of high crystalline quality. The cross-section TEM lamella was prepared along the waveguide axis (parallel view), and gives a good overview of the epitaxial quality along the length of the waveguide (for more TEM analysis, including a TEM lamella prepared perpendicular to the waveguide axis, see Supplementary Section I). The total thickness of the InP-on-Si layer is 515 nm (from the top surface to the bottom of the silicon V-groove). Except for the first 20-nm-thick dark layer at the InP–Si interface and some stacking faults along the trench originating from the complex growth process, hardly any dislocations can be found in the material. This bottom 20-nm-thick defective InP layer is formed during the early stage of the epitaxy process²⁷ and accommodates the entire lattice mismatch, allowing fully relaxed and threading dislocation-free InP material to be grown on top of it. Careful analysis of the optical modes supported by this waveguide (Supplementary Section II) shows that the fundamental optical mode exhibits only limited overlap with this defective layer and is mainly located in the high-quality upper region of the ridge. The damage induced by the CMP process at the top of the ridge in principle could be removed by a soft wet etching process³³, providing room for future performance improvement. Occasionally, we find extended planar defects, for example, micro-twins and stacking faults (SFs) in the bulk region of the waveguide. These are believed to be formed when the growth fronts of two spatially separated nucleation sites coalesce. However, photoluminescence measurements (Supplementary Section III) show no emission from the sub-bandgap states typically associated with such defects, proving the high quality of the material.

Besides the lattice mismatch, the polarity mismatch between the InP and Si could lead to additional defects through the formation of anti-phase boundaries (APBs), which can extend vertically towards

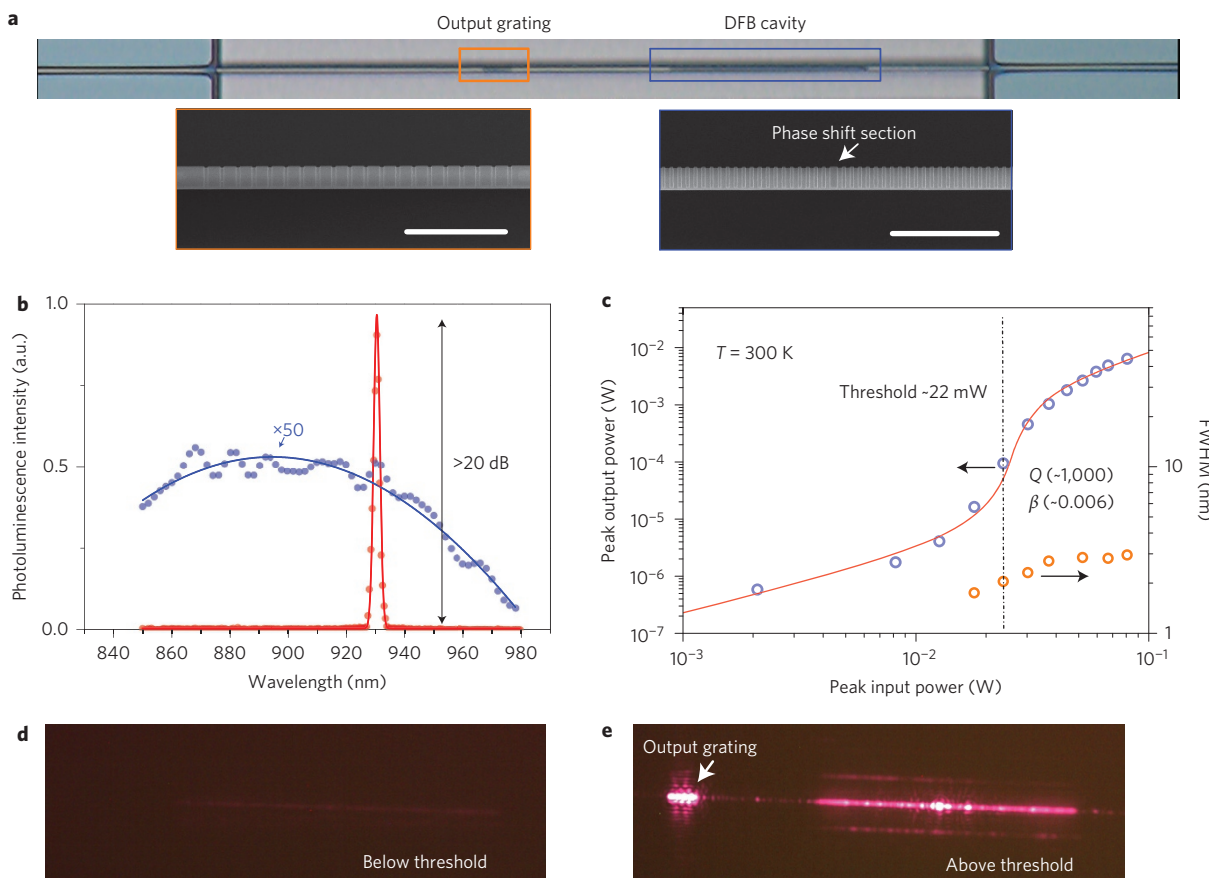


Figure 2 | Laser operation in a single monolithically integrated laser. **a**, Microscope image of a suspended DFB laser grown on a Si substrate. The DFB cavity and the output gratings are outlined by rectangles. Inset: SEM images of the DFB cavity and the output grating. Scale bars, 2 μm . **b**, Room-temperature laser emission spectra measured below (blue) and above (red) threshold. Symbols are measured data and lines are Gaussian fits. **c**, Light in-light out (L-L) curve of the measured DFB laser. Symbols are measured data, and the line is the rate equation fit. A spontaneous emission factor of $\beta \approx 0.006$ is extracted. **d,e**, Camera-recorded photoluminescence images of the laser cavity below and above threshold, respectively.

the top surface^{34,35}. By initiating the growth from the flat $\langle 111 \rangle$ Si planes at the bottom of the trench, the formation of such anti-phase domains is prevented, and TEM images show that the grown InP is indeed APB-free²⁹.

After hetero-epitaxial growth, the 300 mm silicon wafer was diced into small dies for further processing (steps iii to v in Fig. 1f). Initial characterization showed that InP waveguides aligned along the $[011]$ and $[0-11]$ directions performed in a similar manner, so we did not intentionally choose waveguides along a particular direction for laser demonstration. Fabrication commenced with the definition of the gratings in the InP waveguides by electron beam lithography (EBL) and inductively coupled plasma (ICP) dry etching. A carefully optimized isotropic reactive ion etching (RIE) process was then used to remove the silicon substrate below the lasers (see Methods). By avoiding wet etching processes, the 200- μm -long, 500-nm-wide InP waveguides show no collapse onto the substrate. Although, in this work, EBL was used for definition of the gratings, the critical dimensions (80 nm in this case) are achievable using the deep ultraviolet lithography widely used in the CMOS industry (critical dimensions below 50 nm), thus inhibiting in no way scaling up the fabrication to high volumes.

A monolithically integrated InP DFB laser on silicon

Although the diamond-shaped InP waveguide (Fig. 1c) supports multiple transverse modes, the large effective index difference between the fundamental mode and higher-order modes makes it possible to design a DFB cavity supporting single-mode lasing (for a detailed mode analysis see Supplementary Section II). The

fabricated structures were simulated using a three-dimensional finite-difference time-domain (3D-FDTD) method. Figure 3c shows the calculated stop band for a grating etched 60 nm deep in the InP waveguide as a function of its period. The two grey lines denote the lower and upper band edge, respectively. The dashed line in the centre of the band indicates the expected DFB laser operating wavelength, assuming an exact $\lambda/4$ phase shift is introduced³⁶. Based on these simulations we fabricated $\lambda/4$ phase-shifted DFB lasers with a grating period of 163 nm and etch depth of 60 nm. The process was optimized to have a grating duty cycle of 50%. The total cavity length is 45 μm (see microscope and SEM images in Fig. 2a). The grating coupling strength kL was calculated to be 2.87. The lasers were characterized using a micro-photoluminescence ($\mu\text{-PL}$) set-up (see Methods). A 6- μm -wide uniform pumping area defined using a spatial filter fully covers the DFB cavity. Figure 2b shows the photoluminescence spectra of the device optically pumped at room temperature using a Nd:YAG nanosecond pulsed laser (7 ns pulse width, 938 Hz repetition rate). When the pump intensity is low, a broad and noisy spontaneous emission spectrum is measured. By increasing the pump intensity, an optical mode centred at 930.5 nm ultimately reaches more than 20 dB above the background, clear evidence of laser operation. When measuring the optical spectrum as a function of the pump power (Supplementary Section IV), clamping of the background spontaneous emission level is found, indicating clamping of the carrier density above threshold, another strong indication of laser operation. Figure 2c plots the peak output

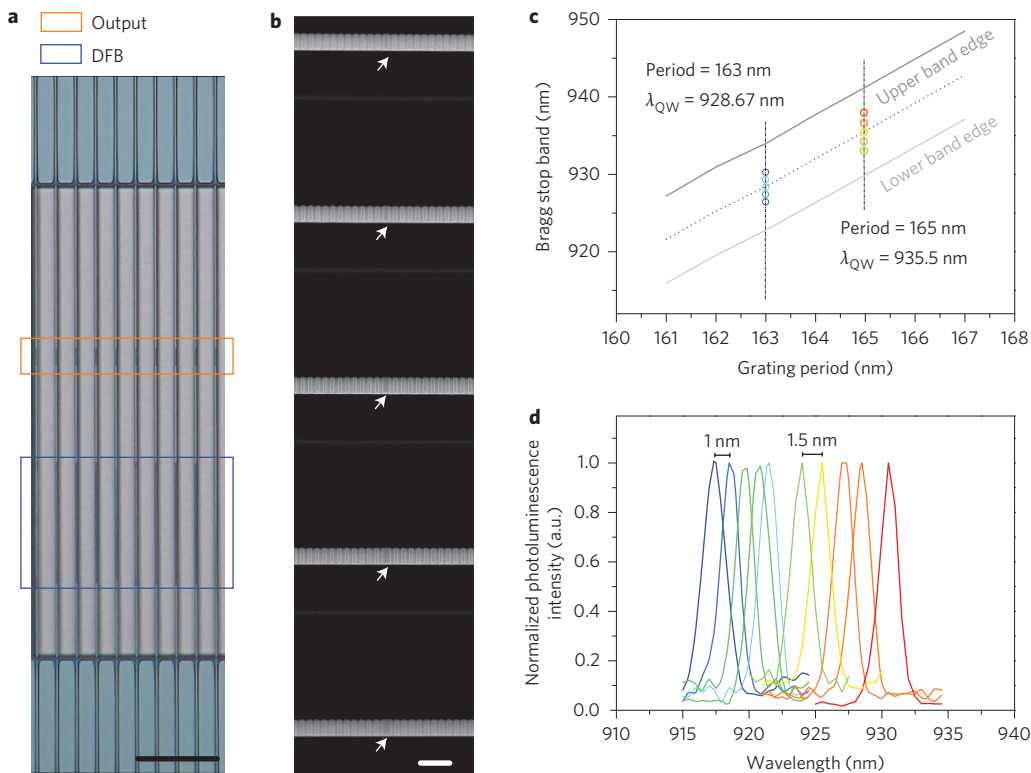


Figure 3 | DFB laser array with lithographically controlled emission wavelengths. **a**, Optical microscope image of the InP-on-Si DFB laser array. The DFB cavities and output gratings are outlined by rectangles. Scale bar, 20 μm . **b**, SEM image of five parallel DFB lasers with the same grating period. The length-varying phase-shift sections are indicated by arrows. Scale bar, 1 μm . **c**, Calculated Bragg stop bands of the DFB grating. A grating etch depth of 60 nm and a 50% duty cycle were used for simulations. Changing the length of the central phase-shift section shifts the lasing wavelength within the stop band, as schematically represented by the coloured dots for the two grating periods used (163 nm and 165 nm). **d**, Measured lasing spectra from the DFB laser array shown in **a**, demonstrating the capability to control the laser wavelength via the grating design.

power as a function of the peak pump power on a logarithmic scale (L-L curve). To estimate the peak power, we assumed the power level to be constant during the 7 ns pulse, and the measured output power was carefully calibrated to include the photoluminescence set-up system loss, the coupling efficiency of the second-order grating and the transmission through the waveguide from the DFB laser to the grating (see Supplementary Section VI). The clear discontinuity in the slope of the curve is another strong signature of laser operation. The laser threshold (P_{th}) was determined to be 22 ± 2.1 mW. When increasing the pump intensity to $3P_{\text{th}}$, a peak output power of 6.4 mW was measured, equivalent to an external efficiency of 6%. From a static rate equation fitting model (red solid curve in Fig. 2c), we extracted a spontaneous emission factor β of 0.006 and a cavity quality factor Q of $\sim 1,000$. We suspect that the difference with the calculated ‘cold’ cavity Q factor of 6,000 can be explained by fabrication imperfections degrading the optical performance of the cavity. Figure 2c also shows the full-width at half-maximum (FWHM) of the resonant mode as soon as it arises from the background. Very similar to what was observed in ref. 37, the lasing peak FWHM increases as the pump intensity increases (from 1.6 nm to 2.8 nm). It is well known that wavelength chirp will appear when a semiconductor laser is modulated³⁸. The varying carrier density changes the refractive index and the optical length of the laser cavity, resulting in an emission wavelength that varies throughout the duration of the optical pumping. In the current case, because the Si detector integrates the received signal over the whole pulse duration, the measured spectrum is broadened by the wavelength chirp (see the dynamic rate equation modelling in Supplementary Section V). The calculated

wavelength chirp is on the order of 1 nm, which agrees with the measurement results.

Figure 2d,e presents photoluminescence images of the DFB laser recorded below and above threshold, respectively. While operating below threshold, the low photoluminescence emission from the DFB cavity can barely be seen. Above threshold (Fig. 2e), a bright spot appears in the centre of the DFB cavity. The spatially concentrated mode profile is indicative of the dominance of the defect mode oscillation in this strongly coupled $\lambda/4$ -shifted DFB laser ($\kappa L = 2.87$). At the left side of the picture the output grating, which is invisible in the below-threshold picture, is now also very bright, and the complex light diffraction indicates the emission of coherent light.

The influence of possible surface damage introduced by the soft dry Si under-etching process was evaluated by comparing photoluminescence spectra taken before and after etching. Neither in the photoluminescence intensity nor in the photoluminescence FWHM was any degradation found. Given the orders of magnitude lower surface recombination velocity of InP compared to most other III-V materials³⁹, the demonstrated laser cavity is very robust against non-radiative surface recombination and requires no extra passivation layers to achieve efficient laser oscillation. To the best of our knowledge, this is the first time an in-plane InP laser has been directly grown on Si without a buffer layer, which is essential for facilitating the coupling of light towards achieving photonics circuits defined on the same wafer, because it allows for perfect vertical alignment of the different waveguide layers.

A monolithic DFB laser array

The high bandwidth provided by WDM could make future optical interconnects far superior to their electronic counterparts⁶ or

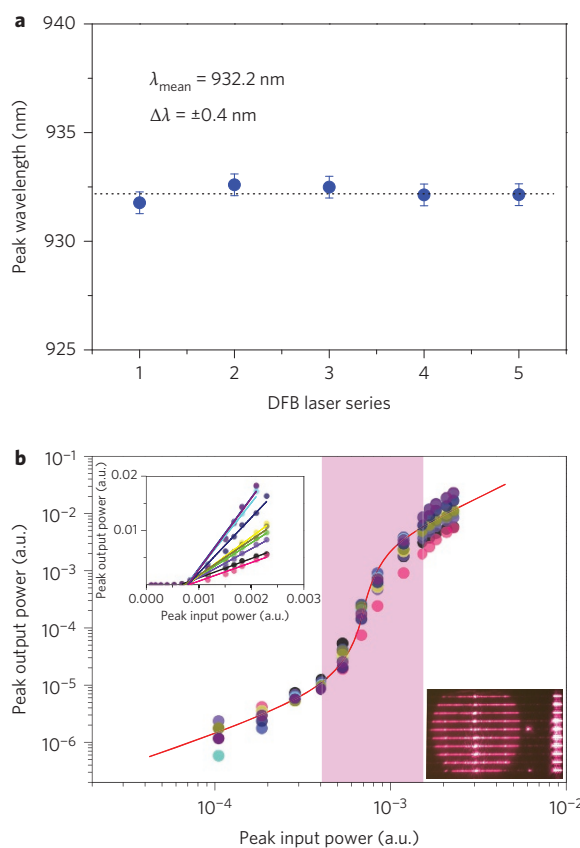


Figure 4 | High yield and scalability of the Si integrated laser array. **a**, Peak lasing wavelengths extracted from the measured lasing spectra of five identical DFB lasers under the same pump intensity. Error bars: inaccuracy introduced by the fitting procedure. **b**, Measured L-L curves of an array of ten DFB lasers. Different colours corresponds to different L-L curves. The S-shaped curve indicated by the solid red line is obtained by rate equation fitting of the averaged output photoluminescence intensity over ten lasers at each pump intensity. Inset (top): linear-scale version of the ten log-scale L-L curves presented in the main panel. Inset (bottom): camera-recorded photoluminescence image of ten working lasers under a large-area pumping condition.

currently deployed single-wavelength optical links. Laser arrays with good wavelength control are thus highly in demand. Here, we demonstrate a monolithically integrated InP DFB laser array on Si. The most straightforward way to tune the operating wavelength of a DFB laser is to vary its grating period. However, as can be seen from Fig. 3c, the latter must be controlled very accurately to achieve narrow wavelength spacing. For example, for a 1 nm wavelength step, the grating period variation will be less than half a nanometre, requiring advanced lithography techniques. To relax the requirements for the lithography tool, instead of altering the grating period, the length of the phase shift section has been altered, in steps of 20 nm away from the exact $\lambda/4$ phase shift length. This small perturbation will cause a shift of the resonant wavelength within the range of the Bragg stop band (see the open circles in Fig. 3c). Figure 3a presents an optical microscope image of a Si integrated InP DFB laser array consisting of ten lasers divided into two groups, with grating periods of 163 nm and 165 nm, respectively. The superimposed laser emission spectra are plotted in Fig. 3d, normalized to peak power. The lasers with 163 nm and 165 nm grating periods show uniform wavelength spacings of 1 nm and 1.5 nm, respectively. The small deviation of the lasing wavelength from the theoretical design (Fig. 3c) can be attributed to fabrication

errors in the grating duty cycle or other geometrical parameters. To the best of our knowledge, this is the first time a precisely controlled in-plane laser array has been monolithically integrated on Si, which is very promising for the realization of high-bandwidth communication systems requiring WDM.

The high yield—at least 98% of over 200 characterized devices showed laser operation—proves the quality of the material and the stability of the laser operation. To illustrate this further, a laser array consisting of five devices with constant grating parameters (165 nm period, 60 nm etching depth, exact $\lambda/4$ phase shift) was fabricated. All five devices show laser operation (the extracted laser operating wavelengths are plotted in Fig. 4a). The small deviation in laser wavelength between the devices is believed to originate from the EBL tool. Figure 4b presents the measured L-L curves (scattered dots) for a second array of ten lasers with similar grating strengths. The bottom right inset in Fig. 4b shows a camera-recorded photoluminescence image of ten working lasers under a large-area pumping condition. The bright spots originate from the grating couplers used to efficiently extract light from the InP waveguides. In the main panel of Fig. 4b, each colour represents a particular laser. The S-shaped curve indicated by the solid red line is obtained by rate equation fitting of the averaged output photoluminescence intensity for ten lasers at each pump intensity. Apart from one L-L curve (pink), the data for the ten different lasers are quite consistent for the spontaneous emission region and the lower part of the amplified spontaneous emission (ASE) region, but the data are a bit scattered in the higher pump intensity region, showing the threshold indeed varies for different lasers. The linear-scale version of the measured L-L curves is shown in the upper left inset of Fig. 4b. The slope efficiency varies for different lasers, but, except for the pink curve, which may just enter the lasing region, all the other curves clearly present the threshold behaviour discussed above, and one can conclude that lasing with good uniformity has been achieved.

Discussion

We have presented a monolithic integration platform that is promising for large-scale, high-volume integration of III-V lasers on silicon. Because the selective-area epitaxy method used here does not limit the length of the active area, traditional and well-understood laser configurations such as Fabry-Perot, distributed Bragg reflector (DBR) and DFB type cavities can be easily adopted. This is a tremendous step forward when compared with nanowire-based devices, for example. Both the limited cavity volume and the complex integration scheme make the latter less attractive for practical applications⁴⁰. Furthermore, because no thick buffer layer is required and the light is emitted in the plane of the wafer, one could envisage butt-coupling the proposed lasers with optical waveguides defined at the same level.

A next critical step towards a practically useful laser will be demonstrating electrical injection and shifting the emission wavelength, allowing the use of Si waveguide structures. Again, the in-plane laser configuration employed makes it straightforward to adopt well-studied electrical injection schemes. The missing element is thus the availability of narrow-bandgap ternary or quaternary compound semiconductors that allow confinement of the injected carriers and redshift the emission wavelength. This road-block can be resolved by using the InP as a buffer on which heterostructures, quantum wells or even quantum dots can be grown, making this virtual InP substrate a powerful platform for various applications. Growth of InGaAs on such virtual InP substrates has already been demonstrated, but the optical quality of the material remains to be proven²⁸. In addition, the use of heterostructures will significantly reduce carrier diffusion into the defective InP/Si interface, suppressing non-radiative recombination and improving the pumping efficiency further.

Finally, the Si substrate undercut process used here was mainly needed to avoid high leakage loss towards the substrate. Growing the III–V waveguide on silicon-on-insulator (SOI) wafers, where the SiO_2 buffer underneath can effectively isolate the optical mode from the substrate, could solve this issue. In addition, direct contact of the III–V lasers with SOI will improve the thermal dissipation of the device, boosting its performance. This also forms a route towards electrical injection for the device.

Processing these devices in an advanced CMOS foundry requires putting in place measures to avoid contamination impacting the performance of other devices processed in the foundry. Recent research demonstrating the full processing of III–V based FinFET devices in a CMOS line^{28,41} demonstrates this is certainly feasible, and the increasing interest of the CMOS industry in III–V based high-mobility channel materials^{16,24} will ensure that more and more foundries will be able to process such devices in the future.

In summary, we have presented the first highly scalable monolithic solution to the long-awaited missing piece of Si photonics: integrated laser sources on Si. The in-plane configuration and the use of a selective-area growth technique directly on 300 mm (001)-Si substrates in combination with a top-down integration scheme provide a route towards the integration of dense arrays of III–V laser sources with Si photonic circuits. A wide range of applications from various fields requiring low-cost on-chip laser sources could benefit from this. In particular, for on-chip optical interconnects, the demonstrated monolithic laser array, together with the WDM technology, may finally pave the way to terascale computing.

Methods

Methods and any associated references are available in the online version of the paper.

Received 7 January 2015; accepted 22 September 2015;
published online 26 October 2015

References

- Liu, A. *et al.* A high-speed silicon optical modulator based on a metal–oxide–semiconductor capacitor. *Nature* **427**, 615–618 (2004).
- Xu, Q., Schmidt, B., Pradhan, S. & Lipson, M. Micrometre-scale silicon electro-optic modulator. *Nature* **435**, 325–327 (2005).
- Assefa, S., Xia, F. & Vlasov, Y. A. Reinventing germanium avalanche photodetector for nanophotonic on-chip optical interconnects. *Nature* **464**, 80–84 (2010).
- Michel, J., Liu, J. F. & Kimerling, L. C. High-performance Ge-on-Si photodetectors. *Nature Photon.* **4**, 527–534 (2010).
- Soref, R. The past, present, and future of silicon photonics. *IEEE J. Sel. Top. Quantum Electron.* **12**, 1678–1687 (2006).
- Miller, D. A. B. Device requirements for optical interconnects to silicon chips. *Proc. IEEE* **97**, 1166–1185 (2009).
- Gunn, C. CMOS photonics for high-speed interconnects. *IEEE Micro.* **26**, 58–66 (2006).
- Ohashi, K. *et al.* On-chip optical interconnect. *Proc. IEEE* **97**, 1186–1198 (2009).
- Fang, A. W. *et al.* Electrically pumped hybrid AlGaInAs–silicon evanescent laser. *Opt. Express* **14**, 9203–9210 (2006).
- Van Campenhout, J. *et al.* Electrically pumped InP-based microdisk lasers integrated with a nanophotonic silicon-on-insulator waveguide circuit. *Opt. Express* **15**, 6744–6749 (2007).
- Liu, L. *et al.* An ultra-small, low-power, all-optical flip-flop memory on a silicon chip. *Nature Photon.* **4**, 182–187 (2010).
- Rong, H. *et al.* A continuous-wave Raman silicon laser. *Nature* **433**, 725–728 (2005).
- Liu, J. F., Sun, X. C., Camacho-Aguilera, R., Kimerling, L. C. & Michel, J. Ge-on-Si laser operating at room temperature. *Opt. Lett.* **35**, 679–681 (2010).
- Takahashi, Y. *et al.* A micrometre-scale Raman silicon laser with a microwatt threshold. *Nature* **498**, 470–474 (2013).
- Wirths, S. *et al.* Lasing in direct-bandgap GeSn alloy grown on Si. *Nature Photon.* **9**, 88–92 (2015).
- ITRS. *International Technology Working Groups International Technology Roadmap for Semiconductors* (2010); <http://www.itrs.net/>
- Ayers, J. E. *Heteroepitaxy of Semiconductors – Theory, Growth, and Characterization* (CRC, 2007).
- Hossain, N. *et al.* Reduced threshold current dilute nitride Ga(NAsP)/Ga quantum well lasers grown by MOVPE. *Electron. Lett.* **47**, 931–933 (2011).
- Reboul, J. R., Cerutti, L., Rodriguez, J. B., Grech, P. & Tournie, E. Continuous-wave operation above room temperature of GaSb-based laser diodes grown on Si. *Appl. Phys. Lett.* **99**, 121113 (2011).
- Chen, S. M. *et al.* 1.3 μm InAs/GaAs quantum-dot laser monolithically grown on Si substrates operating over 100 °C. *Electron. Lett.* **50**, 1467–1468 (2014).
- Wang, T., Liu, H., Lee, A., Pozzi, F. & Seeds, A. 1.3- μm InAs/GaAs quantum-dot lasers monolithically grown on Si substrates. *Opt. Express* **19**, 11381–11386 (2011).
- Chen, R. *et al.* Nanolasers grown on silicon. *Nature Photon.* **5**, 170–175 (2011).
- Wang, Z. *et al.* Polytypic InP nanolaser monolithically integrated on (001) silicon. *Nano. Lett.* **13**, 5063–5069 (2013).
- del Alamo, J. A. Nanometre-scale electronics with III–V compound semiconductors. *Nature* **479**, 317–323 (2011).
- Guo, W. *et al.* Selective metal–organic chemical vapor deposition growth of high quality GaAs on Si(001). *Appl. Phys. Lett.* **105**, 062101 (2014).
- Merckling, C. *et al.* Selective-area metal organic vapor-phase epitaxy of III–V on Si: what about defect density? *ECS Trans.* **64**, 513–521 (2014).
- Merckling, C. *et al.* Heteroepitaxy of InP on Si(001) by selective-area metal organic vapor-phase epitaxy in sub-50 nm width trenches: the role of the nucleation layer and the recess engineering. *J. Appl. Phys.* **115**, 023710 (2014).
- Waldron, N. *et al.* InGaAs gate-all-around nanowire devices on 300mm Si substrates. *IEEE Electron. Device Lett.* **35**, 1097–1099 (2014).
- Paladugu, M. *et al.* Site selective integration of III–V materials on Si for nanoscale logic and photonic devices. *Cryst. Growth Des.* **12**, 4696–4702 (2012).
- Mitsuru, S., Hidefumi, M., Yoshiro, I., Yoshihisa, S. & Masami, T. 1.5 μm -long-wavelength multiple quantum well laser on a Si substrate. *Jpn J. Appl. Phys.* **30**, 3876 (1991).
- Yang, J. & Bhattacharya, P. Integration of epitaxially-grown InGaAs/GaAs quantum dot lasers with hydrogenated amorphous silicon waveguides on silicon. *Opt. Express* **16**, 5136–5140 (2008).
- Liu, H. Y. *et al.* Long-wavelength InAs/GaAs quantum-dot laser diode monolithically grown on Ge substrate. *Nature Photon.* **5**, 416–419 (2011).
- Boroditsky, M. *et al.* Surface recombination measurements on III–V candidate materials for nanostructure light-emitting diodes. *J. Appl. Phys.* **87**, 3497 (2000).
- Cohen, D. & Carter, C. B. Structure of the (110) antiphase boundary in gallium phosphide. *J. Microsc.* **208**, 84–99 (2002).
- Narayanan, V., Mahajan, S., Bachmann, K. J., Woods, V. & Dietz, N. Antiphase boundaries in GaP layers grown on (001) Si by chemical beam epitaxy. *Acta Mater.* **50**, 1275–1287 (2002).
- Coldeen, L. A., Corzine, S. W. & Mashanovitch, M. L. *Diode Lasers and Photonic Integrated Circuits* 2nd edn (Wiley, 2012).
- Tatebayashi, J. *et al.* Room-temperature lasing in a single nanowire with quantum dots. *Nature Photon.* **9**, 501–505 (2015).
- Koch, T. L. & Bowers, J. E. Nature of wavelength chirping in directly modulated semiconductor lasers. *Electron. Lett.* **20**, 1038–1040 (1984).
- Casey, H. C. & Buehler, E. Evidence for low surface recombination velocity on n-type InP. *Appl. Phys. Lett.* **30**, 247 (1977).
- Duan, X., Huang, Y., Agarwal, R. & Lieber, C. M. Single-nanowire electrically driven lasers. *Nature* **421**, 241–245 (2003).
- Waldron, N. *et al.* An InGaAs/InP quantum well FinFET using the replacement fin process integrated in an RMG flow on 300 mm Si substrates. *IEEE Symposium on VLSI Technology 2014: Digest of Technical Papers* 1–2 (2014).

Acknowledgements

This work was supported by the European Commission through ERC project ULPPIC (Ultra Low Power Photonic IC) and imec's industry-affiliation programme on optical I/O. The authors thank R. Baets, G. Roelkens and N. Le Thomas for discussions.

Author contributions

D.V.T. proposed and coordinated the overall project. J.V.C., Z.W. and P.A. suggested the idea of an in-plane laser on silicon. B.T. explored the theoretical design. Z.W. developed the process flow. C.M. and W.G. carried out the epitaxial growth. M.P. processed the silicon template. B.T. and Z.W. performed the photoluminescence characterizations. Z.W. and D.V.T. composed the manuscript.

Additional information

Supplementary information is available in the online version of the paper. Reprints and permissions information is available online at www.nature.com/reprints. Correspondence and requests for materials should be addressed to D.V.T.

Competing financial interests

The authors declare no competing financial interests.

Methods

InP epitaxial growth on pre-patterned silicon wafer. Standard SiO₂ STI patterning was applied on 300 mm on-axis Si (001) substrates to realize 250-nm-thick ridges buried in the SiO₂ buffer. The subsequent selective etching of Si by tetramethylammonium hydroxide (TMAH) solution resulted in trenches with widths ranging from 40 nm to 500 nm. The average active area exposed to the III–V layers deposition was kept constant at 10% of the total Si wafer surface. The trenches were aligned along the [110] and orthogonal [-110] directions, and because the substrate was on-axis there was no difference in the final epitaxial quality between two trench directions. The III–V heteroepitaxy was performed in a 300 mm production AIXTRON Crius metal organic vapor phase epitaxy reactor, equipped with a vertical showerhead injector. The group III precursors in the tool were trimethylindium (TMIn), trimethylgallium (TMGa) and trimethylaluminium (TMAl), and the group V sources were tertiarybutylarsine (TBAs) and tertiarybutylphosphine (TBP). During growth, the reactor pressure varied from 50 mbar to 500 mbar with a H₂ total flow of 48 standard litres per minute as the carrier gas. The native oxide from the trench bottom surface was first thermally desorbed by a high-temperature bake above 800 °C in H₂ at 50 mbar. The substrate temperature was then cooled to a low temperature (<380 °C) to grow the nucleation layer. Below 550 °C, the surface was exposed to As at high pressure to form a one-monolayer As-terminated surface (to promote InP wetting at low temperatures). After the nucleation step, the temperature was ramped up to 550 °C to obtain a high-crystalline-quality InP layer.

InP laser array process flow. To fabricate the suspended DFB laser array on silicon, EBL was used to define the DFB gratings together with the λ/4 phase shift on the InP waveguide. The grating pattern was then transferred by RIE to the 20-nm-thick SiO₂

hard mask, which was deposited by PECVD before the EBL process. The subsequent ICP etching process further transferred the grating pattern to the InP waveguide. After dipping the sample in a 2% HF solution for 20 min to remove the STI oxide mask and expose the silicon substrate, another 200-nm-thick SiO₂ hard mask was deposited on the sample by PECVD. Optical lithography was then used to define 50-μm-wide resist strips at both ends of the DFB cavity, without overlapping on the predefined gratings. A RIE SiO₂ etch process was used to transfer the resist pattern into the 200 nm SiO₂ hard mask and, after removing the resist residuals, the exposed Si substrate under the DFB laser was undercut to 3 μm by an isotropic RIE etching process. No collapse or breakdown of the suspended InP cavity was observed after this RIE Si etching process.

Laser characterization. The laser measurements were carried out at room temperature, without the use of a cryostat or substrate temperature controller. For laser operation, 7 ns pump pulses from a Nd:YAG nanosecond pulsed laser (Ekspla, 532 nm, repetition rate 938 Hz) were delivered to the sample surface by a ×50, 0.65 numerical aperture objective (Mitutoyo NIR HR). The use of optical attenuators together with a half-wave plate and an optical polarizer allowed continuous tuning of the pump power intensity. In addition, the optical set-up was designed to deliver a rectangular uniform pump pattern that fully covers the whole DFB cavity without any overlay on the adjacent devices. The DFB laser emission was collected by the same objective used for pump delivery and detected through a 0.25 m monochromator (MS257, Newport) by a thermoelectric-cooled Si detector. Filters were used to block the pumping light from reaching the detectors. The detector signal was locked by a lock-in amplifier to improve the signal-to-noise ratio.